Ab initio calculation of the O-K, N-K, Si-K, Si-L_3, Y-K, Y-L_3 edges in the Y-Si-O-N system: A strategy for ELNES/XANES spectral modeling in complex materials

W. Y. Ching* and Paul Rulis
Department of Physics, University of Missouri-Kansas City, Kansas City, Missouri 64110, USA
(Received 26 September 2007; published 18 January 2008)

The electron energy-loss near-edge structure (ELNES) or the x-ray absorption near-edge structure (XANES) spectra of the anion (O, N) and cation (Si,Y) (O-K, N-K, Si-K, Si-L_3, Y-K, and Y-L_3) edges in 12 crystals of the Y-Si-O-N system have been calculated using an *ab initio* supercell method based on density functional theory in its local approximation. The collection consists of six binary (α-SiO_2, stishovite SiO_2, β-Si_3N_4, α-Si_3N_4, γ-Si_3N_4, and Y_2O_3), three ternary (Si_2N_2O, $Y_2Si_2O_7$, and Y_2SiO_5), and three quaternary ($Y_2Si_3N_4O_3$, $Y_4Si_2O_7N_2$, and $Y_3Si_5N_9O$) crystals. The calculations took into account the core-hole effect and included the explicit evaluation of the transition matrix elements. Based on the extensive data calculated, attempts were made to correlate the spectral features in the calculated spectra with the local structural environments of the atoms in the crystal. It is shown that with the exception of the fourfold tetrahedrally coordinated Si ion, there is no clear evidence of trends in the ELNES/XANES spectra that can be established to justify a so-called finger printing capability. In crystals with well-defined Si-O_4 units, very different Si-K edges were obtained. For the O-K and N-K edges, there are numerous counterexamples of such a correlation that can be traced to effects beyond the nearest neighbor coordination. In the Y-K and Y-L_3 edges, no meaningful correlations can be established because of the longer bond lengths and more ionic nature of the bonding. For simpler crystals where nonequivalent sites of a particular ion exist, the weighted sum of the spectra from individual sites should be used for comparison with experiment. These results indicate that for proper interpretation of the experimentally measured spectra in complex ceramics, or for ceramic materials containing microstructures, calculated spectra based on simpler crystals with similar coordination should not be used. It is argued that the proper way to understand these spectra would be to actually model the structure and then carry out the full spectral calculations on the constructed models.

DOI: 10.1103/PhysRevB.77.035125 PACS number(s): 78.70.Dm, 79.20.Uv, 78.20.Bh, 78.66.Nk

I. INTRODUCTION

In recent years, electron energy-loss spectroscopy (EELS) has developed into a very versatile tool for materials characterization,[1–5] especially with complex systems containing microstructure, interfaces, internal grain boundaries, etc. It has often been claimed that EELS and the associated spectra in the near edge, electron energy-loss near-edge structure (ELNES), can reveal the detailed electronic structure and bonding in such materials. Recent improvements in instrumentation with other various corrections have pushed the energy resolution to the level of 0.2 eV and beyond.[6,7] In practice, such a lofty goal has not been achieved except in simple crystals where the atomic bonding is relatively simple. The typical examples are the σ^* and π^* bondings in graphite that differ from sp^3 bonding in diamond crystal.[8] In most cases, the experimentally measured spectra for the same edge focusing on different spots of a structurally complicated sample differ only in minor details, making proper analysis relating to local structure a daunting task. This is mainly because the ELNES measurements are beam sensitive and have an illuminated sample area larger than the atomic scale resolution. Experimental data are also subject to background subtraction for the tail of the strong zero-loss peak. Different practices and techniques by different groups also add some uncertainty.

The availability of intense light sources in the form of synchrotron radiation from storage rings all over the world within the past decades has promoted the x ray as the primary source for studying the electronic structure and bonding in materials. The x-ray absorption near-edge structure (XANES) (also named as near-edge x-ray absorption fine structure) is, in principle, similar to ELNES except that it uses intense x rays as the source and, therefore, can probe at a much higher energy range compared to ELNES. However, ELNES has an advantage in that it contains information on both energy and momentum transfer, while XANES has only the energy transfer. In the limit of low momentum transfer, these two techniques can be considered similar to each other. ELNES is measured by using high resolution transmission electron microscopy or scanning transmission electron microscopy, and has the advantage of high spatial resolution. ELNES can be measured at near normal vacuum conditions and is not particularly sensitive to the surface. XANES has the advantage of high intensity, high energy resolution, a small divergence of the beam, and is the preferred technique to study materials with heavy elements including the rare earth and transuranic elements.

The interpretation of the ELNES/XANES spectra has been greatly facilitated by comparing the measured spectra with theoretically calculated ones. In the past three decades, many theoretical and simulation methods have been developed for this purpose. Initially, the agreement between the measured and the calculated spectra were poor and the computational techniques were far from being predictive. Most of these calculations were devoted to either one or two specific crystals with simple crystal structures, or were focused on a given edge with total disregard for the other edges in the

same crystal. In many of these works,[9–14] the "finger printing" technique was used to distinguish a few well-defined local environments of the ions. Within the past decade or so, significant development of theoretical tools has greatly improved the quality of the calculated XANES/ELNES spectra, and, in some cases, predictability is a realistic goal.[15–23] Still, for complicated multicomponent systems, such predictability is far from being clear and a different strategy and approach need to be developed.

In this paper, we present detailed calculations of the ELNES/XANES spectra of all elements in the 12 crystals within the general Y-Si-O-N system. The electronic structure and bonding of these crystals have been reviewed in a recent series of papers.[24–29] Our goal is to use the Y-Si-O-N system, in which a variety of bonds between cations (Y,Si) and anions (O,N) exist, to develop a general rule (or lack thereof) for interpreting ELNES/XANES spectra based on local nearest neighbor (NN) coordination that would be useful for the modeling of complex nanostructured ceramic materials. We would also like to use this comprehensive set of data, calculated using a state-of-the-art method, to refute some prevailing concepts and questionable assumptions regarding the interpretations of the ELNES/XANES spectra. Our results provide a database of high quality ELNES/XANES spectra that can be used for comparison with data obtained from future measurements or from calculations using other methods. The majority of the spectra presented in this paper have no experimental data to compare with at this moment and can be considered as predictions.

We used the now well-established supercell orthogonalized linear combination of atomic orbitals (OLCAO) method[30] at the level of density functional theory (DFT) in its local density approximation (LDA) for ELNES/XANES spectral calculations. Since the first publication of the OLCAO-supercell approach, the method has been successfully applied to many crystals,[15–20,30–34] defects,[23,35,36] interfaces,[37] and grain boundary structures[21,22,38] in ceramics with results in good agreement with experiments. The present calculations are very comprehensive, comprising the O-K, N-K, Si-K, Si-L_3, Y-K, and Y-L_3 edges in 12 crystals (α-SiO_2, stishovite SiO_2, β-Si_3N_4, α-Si_3N_4, γ-Si_3N_4, Y_2O_3, Si_2N_2O, $Y_2Si_2O_7$, Y_2SiO_5, $Y_2Si_3N_4O_3$, $Y_4Si_2O_7N_2$, and $Y_3Si_5N_9O$). In Ref. 28, for the electronic structure and optical properties, our analysis includes the two other quaternary crystals $YSiO_2N$ and $Y_{10}[SiO_4]_6N_2$ (N-apatite). They are not included in the present study for ELNES/XANES spectra because the structures of these two crystals are not as well established as the other quaternary Y-Si-O-N crystals.[24,26] On the other hand, we have included the N-rich $Y_3Si_5N_9O$ compound in the study because of its unique structure of having only one O ion in the crystal.[29] We have also added the α-Si_3N_4 and γ-Si_3N_4 phases. The high pressure phase γ-Si_3N_4 is particularly illuminating because of the rare occurrence of the octahedral bonding of Si to N.[39,40] The cations and anions in these complex crystals have crystallographically nonequivalent sites and different local coordinations and bonding environments, thus providing a rich playground for seeking meaningful correlations based on calculated site-specific spectra and detailed structural analysis. We consider the local NN and next NN (NNN) environments of both the cations and anions by taking into consideration the number of bonds and the types of bonds (chemical species), and by paying special attention to any noticeable exceptions including bond angles and crystalline anisotropy. We focus on the comparison of the ELNES/XANES spectra of the same element in different local environments. Based on these calculations, specific correlations (or the lack of such correlations) with local structural characteristics in these complex crystals are presented. No specific comparison with experimental data is attempted. This is because for most of the complex crystals studied here, there are no measured data available. For some binary compounds, comparisons of the calculated data with the measured data show excellent agreement, which have been reported in the published literature [α-SiO_2,[19,31] stishovite SiO_2,[19,31] β-Si_3N_4,[32] Si_2N_2O,[32] γ-Si_3N_4,[15,32] and α-Si_3N_4 Ref. 32] and will not be repeated here. For these crystals, the results presented here are the repeated calculations along with the other crystals for consistency.

In the next section, we summarize the local atomic-scale structures around the anions (O, N) and cations (Si, Y) in these 12 crystals. This is followed by a brief description of the method of calculation. The main results are presented in Sec. IV and discussed in Sec. V. The paper ends with a summary in Sec. VI together with our conclusions.

II. BONDING CONFIGURATIONS IN THE BINARY, TERNARY, AND QUATERNARY CRYSTALS

Before we present the method and the results of the ELNES/XANES calculation, we will first analyze the structure and the local bonding configuration of the ions in the 12 crystals. This makes our analysis of the calculated results much easier. In the electronic structure studies, the total density of states (DOS) can be easily resolved into atom specific partial DOS (PDOS). This is a common practice in many electronic structure studies. In the analysis of ELNES/XANES spectra, it is difficult to resolve each edge into partial components of different atoms of the same chemical species since the electronic structure of the empty conduction bands (CBs) are generally more delocalized. In the past, the calculated orbital-resolved PDOS of the CB states were often used to interpret the experimental ELNES/XANES data with only limited success.[42–44] In the analysis of experimental data for complex crystals or structures containing microstructures and defects, it is customary to use the spectra from simpler crystals as a guideline for interpretation. This approach seldom works because the CB states are not a superposition of those from crystals with similar local environments and there are too many unknown factors that affect the unoccupied electronic states. In the present study, we will illustrate this subtle point, which is generally ignored in experimental analysis, by careful analysis and comparison of the vast amount of the data calculated within a single scheme.

In Table I, we list the crystal structures and the space groups of the 12 crystals studied. The list consists of six binary (α-SiO_2, stishovite SiO_2, β-Si_3N_4, α-Si_3N_4, γ-Si_3N_4, and Y_2O_3), three ternary (Si_2N_2O, $Y_2Si_2O_7$, and Y_2SiO_5),

TABLE I. Comparison of crystal structure of the 12 Y-Si-O-N crystals. The supercell size is indicated by the number of the atoms in the cell and lattice multiplicity (in parentheses). N_P is the number of atoms in the primitive cell of the crystal.

Crystal	Lattice constants (Å)	Space group	N_p	Supercell size	Y/(O+N)	Si/(O+N)	O/(O+N)	N(O+N)
α-SiO_2	a=4.916, c=5.405	$P3_221$ (154)	9	72 (2×2×2)		0.5	1.0	
Stishovite	a=4.179, c=2.665	$P4_2$ (136)	6	144 (2×2×4)		0.5	1.0	
β-Si_3N_4	a=7.607, c=2.911	$p6_3/m$ (176)	14	168 (2×2×3)		0.75		1.0
α-Si_3N_4	a=7.766, c=5.615	$p3_1c$ (176)	28	224 (2×2×4)		0.75		1.0
γ-Si_3N_4	a=7.8367	$Fd3m$ (159)	14	112 (2×2×2)		0.75		1.0
Y_2O_3	a=10.6073	Ia-3 (206)	40	80 (cubic cell)	0.666		1.0	
Si_2N_2O	a=8.8742, b=5.4894, c=4.8486	$Cmc2_1$ (36)	10	120 (2×2×3)		0.666	0.333	0.666
$Y_2Si_2O_7$	a=4.694, b=10.856, c=5.588 β=95.01°	$p21/c$ (4)	22	88 (2×1×2)	0.286	0.286	1.0	
Y_2SiO_5	a=14.371, b=6.71, c=10.388 β=122.17°	$C2/c$ (15)	32	128 (1×2×2)	0.40	0.20	1.0	
$Y_2Si_3N_4O_3$	a=7.4238, b=7.6027, c=4.8162 β=89.938°	$P2_1$ (4)	24	192 (2×2×2)	0.286	0.429	0.429	0.571
$Y_4Si_2O_7N_2$	a=7.5601, b=10.4411, c=10.7626 β=110.042°	$P2_1/c$ (14)	60	120 (2×1×1)	0.444	0.222	0.778	0.222
$Y_3Si_5N_9O$	a=4.9697, b=16.1192, c=10.6277	$pbcm$ (57)	72	144 (2×1×1)	0.333	0.50	0.100	0.900

and three quaternary ($Y_2Si_3N_4O_3$, $Y_4Si_2O_7N_2$, and $Y_3Si_5N_9O$) crystals. Even the binary crystals such as Y_2O_3 and α-Si_3N_4 have rather complex structures. Also listed are the supercell sizes used in the OLCAO calculation (see next section). The supercells were chosen such that they will provide accurate ELNES/XANES spectra without being prohibitively time consuming. For the convenience of making a connection to the experimental samples, we have also listed the ratio of each type of ion to the total number of anions (O+N) in these crystals. We next describe the local atomic environment and the number of nonequivalent sites of O, N, Si, and Y in these crystals. They are listed in Tables II–V. These tables contain the structural details of the two anions and two cations in these crystals which will help us to analyze the calculated spectra presented in Sec. IV. In each table for a particular ion, the first column specifies the crystal. The second column lists the number of nonequivalent sites of this ion in the crystal with their ratios in parentheses. The third column lists the number of NN atoms for the ion at each site. In the fourth column, the NN coordination at each site is indicated and the number in parentheses indicates the number of occurrences of this coordination. As an example, in Table II, O-Si2 implies that the O is bonded to two Si ions as NN, and O-SiY3 implies that the O is bonded to one Si and three Y ions. The fifth column lists the NN bond lengths (BLs) of the local coordination. The number in parentheses indicates the occurrence of this BL for the configuration in the fourth column. In a few cases with quaternary crystals, there are too many BLs for the Y ions to be listed. Only the range (minimum to maximum) is indicated.

As can be seen from Tables II–V, there is a plethora of local bonding configurations in the Y-Si-O-N system and their potential role in characterizing the structures in the ELNES/XANES spectra is most interesting. Because of the rather comprehensive list of crystals with different structures in the present investigation, it is unlikely that any other type of NN configurations will occur in other crystals, although we cannot rule them out completely. For the Y ion, the NN analysis is a little uncertain because of a much larger variation in the BL due to the more ionic nature of the Y-O and Y-N bonds. We used the value of 2.95 Å as the upper limit for both Y-O and Y-N BLs.

III. METHOD OF XANES/ELNES CALCULATION

The theory of electron energy-loss spectroscopy based on quantum scattering theory has been reviewed in many papers.[1,45–50] The basic quantity to measure is the inelastic partial differential scattering cross section.

$$\frac{d^2\sigma}{d\Omega dE} = \frac{1}{(\pi e a_0)q^2}\,\mathrm{Im}\left\{\frac{-1}{\varepsilon(\vec{q},\hbar\omega)}\right\}, \tag{1}$$

where $\varepsilon(\vec{q},\hbar\omega)$ is the microscopic complex dielectric function and Im stands for the imaginary part. For small momentum transfer and at energies far above the plasma frequency $\mathrm{Im}\{-1/\varepsilon(\vec{q},\hbar\omega)\} \sim \varepsilon_2(0,\hbar\omega)$, the transition probability I per unit time for the inner shell core excitation in ELNES/XANES within the dipole approximation can be reduced to the following expression according to the Fermi golden rule:[51]

TABLE II. Local O environment in nine Y-Si-O-N crystals. N_O denotes the number of nonequivalent O sites. The ratios of the nonequivalent sites are in parentheses.

Crystal	N_O	NN N_O	NN coordination	NN bond length (Å)
α-SiO_2	1	2	O-Si2	1.605, 1.614
SiO_2 (stishovite)	1	3	O-Si3	1.757 (2), 1.810
Y_2O_3	1	4	O-Y4	2.244, 2.268, 2.288, 2.337
Si_2N_2O	1	2	O-Si2	1.624 (2)
$Y_2Si_2O_7$	4 (1:2:2:2)	2, 3 (3)	O-Si2, O-SiY2	1.631 (2); 1.622, 2.252, 2.274; 1.616, 2.251, 2.297; 1.627, 2.250, 2.328
Y_2SiO_5	5 (1:2:2:2:2)	4, 4, 3 (3)	O-Y4, O-SiY3, O-SiY2 (3)	2.199, 2.203, 2.279, 2.373; 1.628, 2.283, 2.374, 2.604, 1.602, 2.275, 2.319; 1.605, 2.280, 2.287; 1.636, 2.299, 2.317
$Y_2Si_3N_4O_3$	3 (1:1:1)	4, 4, 4	O-Si2Y2, O-SiY3 (2)	1.697, 1.713, 2.355, 2.852; 1.653, 2.359, 1.377, 2.555; 1.630, 2.361, 2.509 (2)
$Y_4Si_2O_7N_2$	7 (1:1:1:1:1:1:1)	4 (7)	O-SiY3 (5), O-Y4 (2)	1.704, 2.271, 2.391, 2.692; 1.621, 2.265, 2.422, 2.621; 1.618, 2.310, 2.336, 2.599; 1.677, 2.285, 2.368, 2.691; 1.600, 2.297, 2.302, 2.902; 2.220, 2.278, 2.297, 2.319; 2.164, 2.248, 2.263, 2.287;
$Y_3Si_5N_9O$	1	4	O-SiY3	1.653, 2.346, 2.494 (2)

$$I \propto \sum_n |\langle g|\vec{r}|f\rangle|^2 \delta(\hbar\omega + E_g - E_f), \quad (2)$$

where g and f stand for the initial ground state and the final state with energies E_g and E_f. The summation in Eq. (2) is over all final states. In the context of one-electron band theory, the initial state g is the ground state of the solid and f are the final states in the empty conduction bands. In the early development of the ELNES/XANES calculation, the matrix elements in Eq. (2) were approximated by the orbital resolved PDOS of the CB with specific angular momentum symmetry using the argument that the core level is highly localized and orthogonal to the final states. The selection rule from the dipole approximation restricts the transition from the $1s$ core state ($\ell=0$) to only the p states ($\ell=1$), and the transition from the $2p$ core state ($\ell=1$) can end up in states with a $(s+d)$ ($\ell=0$ or 2) type of orbital symmetry. In a more advanced treatment such as in the present calculations, the dipole matrix elements are explicitly calculated from the wave functions, and the section rules are automatically imposed by the symmetry of the wave functions. In the supercell OLCAO method, the Bloch functions for the initial and final states are expressed in terms of Bloch sums b which are expanded in terms of atomic orbitals u centered at each atom:[52]

TABLE III. Local N environment in seven Y-Si-O-N crystals. N_N denotes the nonequivalent N sites. The ratios of the nonequivalent sites are in parentheses.

Crystal	N_N	NN N_O	NN coordination	NN bond length (Å)
β-Si_3N_4	2 (3:1)	3, 3	N-Si3 (2)	1.711, 1.758 (2); 1.719 (3)
α-Si_3N_4	4 (3:3:1:1)	3, 3, 3, 3	N-Si3 (4)	1.710, 1.763, 1.773; 1.700, 1.736, 1.758; 1.732 (3); 1.731(3)
γ-Si_3N_4	1	4	N-Si4	1.765, 1.869 (3)
Si_2N_2O	1	3	N-Si3	1.718, 1.722, 1.726
$Y_2Si_3N_4O_3$	4 (1:1:1:1)	4 (4)	N-Si2Y2	1.639, 1.664, 2.282, 2.331; 1.684, 1.692, 379, 2.695; 1.682, 1.700, 2.356, 2.563; 1.686, 1.671, 2.327, 2.768
$Y_4Si_2O_7N_2$	2 (1:1)	4, 4	N-Si2Y2, N-SiY3	1.707, 1.732, 2.330, 2.481; 1.664, 2.315, 2.318, 2.767
$Y_3Si_5N_9O$	6 (2:2:1:2:1:1)	4 (5), 5	N-Si2Y2 (4), N-Si2Y3, N-Si3Y	1.723, 1.745, 2.521, 2.357; 1.723, 1.727, 2.389, 2.439; 1.735 (2), 2.444 (2); 1.718, 1.730, 2.373, 2.820, 2.877; 1.738, 1.770 (2), 2.568

TABLE IV. Local Si environment in 11 Y-Si-O-N crystals. N_{Si} denotes the nonequivalent Si sites. The ratios of the nonequivalent sites are in parentheses.

Crystal	N_{Si}	NN N_O	NN coordination	NN bond length (Å)
α-SiO_2	1	4	Si-O4	1.605 (2), 1.614 (2)
SiO_2 (stishovite)	1	6	Si-O6	1.757 (4), 1.810 (2)
β-Si_3N_4	1	4	Si-N4	1.711, 1.719, 1.758 (2)
α-Si_3N_4	2 (1:1)	4, 4	Si-N4	1.710, 1.731, 1.738, 1.773; 1.700, 1.732, 1.758, 1.763;
γ-Si_3N_4	2 (1:2)	4, 6	Si-N4, Si-N6	1.765 (4), 1.869 (6)
Si_2N_2O	1	4	Si-ON3	1.624, 1.718, 1.722, 1.726
$Y_2Si_2O_7$	1	4	Si-O4	1.616, 1.622, 1.631, 1.637
Y_2SiO_5	1	4	Si-O4	1.602, 1.605, 1.628, 1.636
$Y_2Si_3N_4O_3$	3 (1:1:l)	4, 4, 4	Si-ON3 (2), Si-O2N2	1.713, 1.683, 1.684, 1.686; 1.653, 1.664, 1.692, 1.700; 1.630, 1.697, 1.639, 1.671
$Y_4Si_2O_7N_2$	2 (1:1)	4, 4	Si-O2N2, Si-O3N	1.621, 1.677, 1.664, 1.732; 1.600, 1.618, 1.704, 1.707
$Y_3Si_5N_9O$	4 (1:1:2:1)	4, 4, 4, 4	Si-N4 (3), Si-ON3	1.723 (2), 1.745 (2); 1.653, 1.697, 1.727 (2); 1.718, 1.723, 1.735, 1.770, 1.664, 1.730 (2), 1.738

$$\Psi_{nk}(\vec{r}) = \sum_{i,\alpha} C^n_{i\alpha}(\vec{k}) b_{i\alpha}(\vec{k},\vec{r}), \tag{3}$$

$$b_{i\alpha}(\vec{k},\vec{r}) = \left(\frac{1}{\sqrt{N}}\right) \sum_{v} e^{i\vec{k}\cdot\vec{R}_v} u_i(\vec{r} - \vec{R}_v - \vec{t}_\alpha). \tag{4}$$

In Eqs. (3) and (4), n is the band index, $C^n_{i\alpha}$ is the wave function (in the form of eigenvectors) of the self-consistent solution of the secular equation, (i,α) is a pair of indices specifying the orbital and atomic state, and v is the index for the supercell lattice. For a sufficiently large cell, the Brillouin zone is very small, we can set $\boldsymbol{k}=0$ or the zone center, and the index $\boldsymbol{k}$ in Eqs. (3) and (4) can be dropped. So the dipole matrix in Eq. (2) takes the form

$$\langle g|\vec{r}|f\rangle \rightarrow M_{i\alpha,j\beta} = \langle b_{i\alpha}|\vec{\nabla}|b_{j\beta}\rangle = \sum_{v} \int u_i(\vec{r} - \vec{t}_\alpha)\vec{\nabla} u_j(\vec{r} - \vec{R}_v - \vec{t}_\beta) d\vec{r}. \tag{5}$$

Equation (5) can be easily calculated since the atomic orbitals in the OLCAO method are expressed in terms of Gaussian type orbitals. The two center integrals in Eq. (5) can be evaluated analytically. The explicit inclusion of the dipole transition matrix in the intensity calculation of the ELNES/XANES spectrum is an important component in providing more accurate amplitudes of transitions in the spectral features.

One of the problems in the ELNES/XANES calculation that has been recognized early on is the core-hole effect in insulators.[53–55] In metals, the effective screening by the CB electrons may reduce the core-hole effect significantly.[56,57] When an electron is excited from the inner core shell to the CB of the solid, it leaves behind a core hole (positively charged) which interacts with the excited electron in the CB, a process analogous to the excitonic effect in semiconductors. To minimize the spurious interactions between the positively charged core holes in adjacent supercells, the size of the supercell used must be sufficiently large. Thus, the core-hole effect cannot be accurately accounted for if the calculations of the ELNES/XANES spectra used the primitive cell of the crystal. In the OLCAO supercell scheme, the electron

TABLE V. Local Y environment in six Y-Si-O-N crystals. N_Y denotes the nonequivalent Y sites. The ratios of the nonequivalent sites are in parentheses. For more than four different BLs of the same type, only the maximum and the minimum are indicated.

Crystal	N_Y	NN N_O	NN coordination	NN bond length (Å)
Y_2O_3	2 (1:3)	6, 6	Y-O6 (2)	2.288 (6), 2.244 (2), 2.234 (2); 2.268 (2)
$Y_2Si_2O_7$	1	6	Y-O6	2.250–2.328 (min to max)
Y_2SiO_5	2 (1:1)	7, 6	Y-O7, Y-O6	2.199–2.604 (min to max); 2.203–2.287(min to max)
$Y_2Si_3N_4O_3$	2 (1:1)	8	Y-O3N5, Y-O5N3	2.359, 2.509, 2.555, 2.331–2.768 (min to max for five Y-N bonds) 2.355–2.852 (min to max for five Y-N bonds), 2.282, 2.327, 2.563
$Y_4Si_2O_7N_2$	4 (1:1:1:1)	8, 7, 6, 7	Y-O6N2, Y-O7, Y-O5N, Y-O5N2	2.263–2.902 (min to max for six Y-O bonds), 2.330, 2.767
$Y_3Si_5N_9O$	2 (2:1)	7, 8	Y-ON6, Y-ON7	2.494, 2.324–2.820 (min to max for six Y-N bonds)

core-hole interaction is fully taken into account at the level of the LDA of density functional theory.[58,59] The initial state and the final states are calculated separately by solving the self-consistent Kohn-Sham equations. The initial state is the ground state of the supercell, with the core states of the targeted atom retained in the orthogonalization procedure. The final state is obtained by moving the electron in the core to the lowest CB state, and the resulting Kohn-Sham equation is solved self-consistently. It is assumed that the self-consistent solution of the final state accounts for all the multiple scattering effects of the excited electron in the CB. The interaction of the electron in the CB and the hole left behind greatly modify the final state wave function, and is the single most important factor for the calculation to reproduce the measured spectra.[30] This procedure of accounting for the electron core-hole interaction is superior to the so-called $(Z+1)$ approximation.[60,61] The latter cannot distinguish the effect of the core hole for transitions from different core levels. The final spectrum is obtained by using Eq. (2) with the dipole matrix elements calculated between the initial and final states.

Another advantage of the OLCAO-supercell method is that the transition energy for each edge can be obtained from the difference in the total energies of the ground state (N electrons) and the final state ($N-1$ electrons). Here, the reference to N-electron and $(N-1)$ electron system is in the spirit of the density functional theory even though the actual calculations of the final states involve N electrons, albeit with one of them in the conduction band region. Although the theoretical transition energy can never reproduce the experimental energy at the edge onset and depends on the size of the supercell, it is usually within a few percent of the transition energy and is very useful for the comparison of different spectra of the same edge at different sites or in different crystals as long as the same computational procedure is used in the calculations.

The OLCAO-supercell method has been successfully applied to the calculation of the XANES/ELNES spectra of a large number of crystals as well as systems with microstructures and defects.[15–23,30–41,62–66] More recently, similar supercell calculations have also been used by other groups using different computational methods.[4,67–72] It has been shown that in crystals where nonequivalent sites for the same species of atom exist, the spectra at the different sites of the same element will be different. The experimentally obtained spectra cannot distinguish the data collected from crystallographically nonequivalent sites. It is imperative to use the weighted sum of the calculated spectra at various sites to compare with the measured spectra of a particular edge. The most vivid examples are the recent calculations of the ELNES spectra of sillimanite[33] (Al_2SiO_5) and γ-Si_3N_4.[15] In sillimanite, Al atoms occupy both the tetrahedral sites and the octahedral sites, which have different spectral characteristics. Only the appropriately combined spectrum can achieve good agreement with the measured spectra. The case for γ-Si_3N_4 will be discussed later.

It is not uncommon to apply a broadening procedure to the calculated spectra since the lifetime effect is not included in most of the theoretical formalisms. There are research efforts specifically dedicated to this subject in order to better understand the actual process in the experiments. In the present calculations (and those published previously), all ELNES/XANES spectra are broadened by a Gaussian with a full width at half maximum of 1.0 eV. In other words, no attempts were made to use the broadening procedure itself to achieve better agreement with experiment. For easy comparison, all spectra for the same edge are normalized to the same area. It should also be pointed out that the supercells used in the calculation must be chosen carefully. A small supercell will give inaccurate results because of the considerable interaction between the adjacent core holes. Too large a supercell increases the computational burden. It is not the number of the atoms in the supercell that matters. It is the distance of separation between the core holes of the adjacent supercells that is relevant. Our past experience indicates that a core-hole separation distance of about 8–9 Å is quite sufficient. So, the efficiency of the calculation treats highly anisotropic crystals and those with light elements (shorter bond lengths) unfavorably. The supercells used for the 12 different crystals in the present calculations are listed in Table I.

IV. RESULTS

The results of the calculated ELNES/XANES edges in the 12 crystals are presented in this section. For each edge, we first show the spectra of that edge from the involved crystals so as to have a quick glance at the overall differences among them. These are the spectra that are most relevant for comparison with the measured ones. For those crystals that have nonequivalent sites, the spectrum is the weighted average over these sites. This is then followed by the presentation of individual spectra at each site in crystals with nonequivalent sites. The local NN bonding configurations are indicated in each panel of the figures. We feel that this is the best way to systematically present our vast amount of results in a cohesive way.

A. O-K edges

Figure 1 shows the calculated O-K edges in nine crystals. Five of these have unique O sites, and their local bonding configurations are indicated. The number of nonequivalent O sites in the four crystals is noted in parentheses in Fig. 1 and also in Table II. It is obvious that these spectra are very different, especially in the first 10 eV range from the edge onset, displaying features with double peaks, single broad peaks, additional small peaks, and shoulders. Even for O ions in the bridging configuration O-Si2 [α-SiO_2, Si_2N_2O, and O1 in $Y_2Si_2O_7$ in Fig. 2(a)], the spectra have noticeable differences in their shape and edge onset. This could imply that the O-K edge spectrum may be influenced by the second NNs, bond angles, etc. (The O bridging angle in the three crystals are 143.7°, 150.0°, and 180.0°, respectively.) O in stishovite is the only case where it bonds to three Si atoms. Its spectrum shows a sharp leading peak followed by a prominent but broad peak in the first 10 eV range. O in Y_2O_3 and in $Y_3Si_5N_9O$ both have four NN atoms, with four Y in the former and one Si with three Y in the latter. Their spectra are also very different in the separations of the double peaks

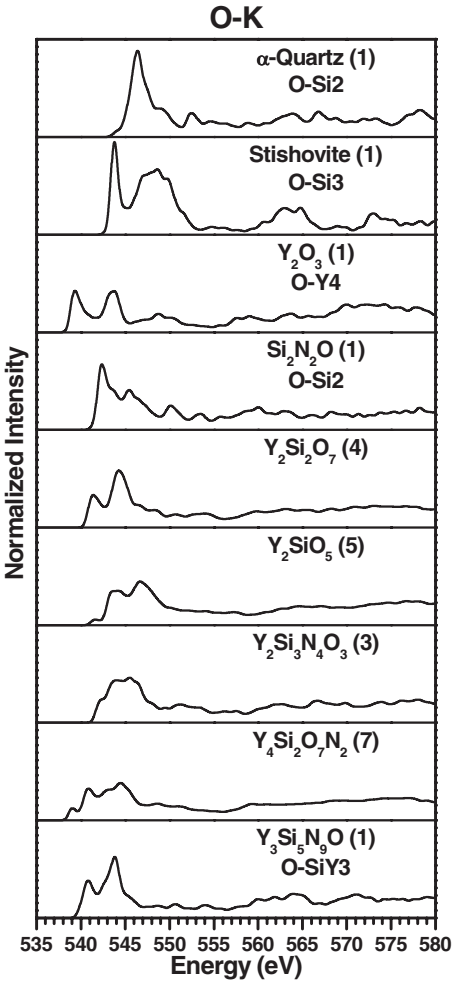

FIG. 1. Calculated total O-K edges in nine crystals. The number in parentheses indicates the number of nonequivalent sites for O. For crystals with unique O site, their NN bonding coordination is indicated.

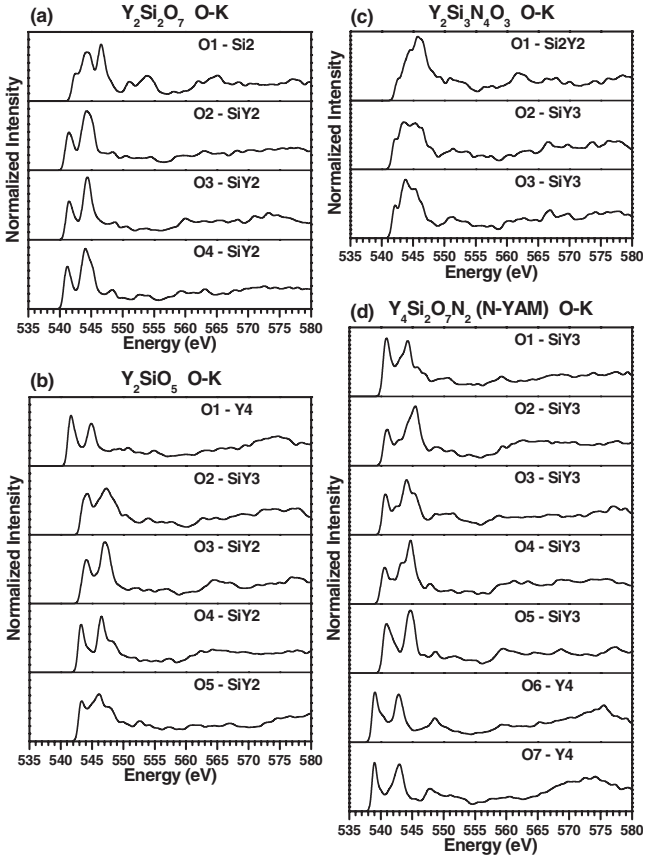

FIG. 2. The site-specific O-K edges in crystals with nonequivalent sites: (a) $Y_2Si_2O_7$, (b) Y_2SiO_5, (c) $Y_2Si_3N_4O_3$, and (d) $Y_4Si_2O_7N_2$. The NN bonding coordination is indicated.

and in their relative intensities. These variations underscore the importance of the chemical species in the NN shell in addition to the NN numbers.

The weight-averaged O-K edges in $Y_2Si_2O_7$, Y_2SiO_5, $Y_2Si_3N_4O_3$, and $Y_4Si_2O_7N_2$ in Fig. 1 are more broadened as expected. They are very different from the crystals with only one O site. In Fig. 2, we display the spectra from the nonequivalent sites in these crystals. In $Y_2Si_2O_7$, the spectrum for O1 in a bridging configuration with two Si atoms is very different from the spectra of O2, O3, and O4, which all bond to one Si and two Y, and whose spectra are very similar with well-defined double peaks. In Y_2SiO_5, O1 distinguishes itself as having four Y as NN and is responsible for a prominent sharp peak at −15.1 eV in the valence band.[25] The spectrum for O1 resembles that of O in Y_2O_3, but with different peak intensities. This could be related to the shorter O-Y bonds in Y_2SiO_5 (see Table II). The spectra of O2 through O5, though having a similar double-peak structure, have higher absorption edges compared to O1. O2 bonds to one Si and three Y, while O3, O4, and O5 all bond to one Si and two Y. For that reason, the second peak in O2 is broader than that in O3 and O4. Conspicuously, the O-K edge of O5 is quite different from O3 and O4 in spite of the same local coordination. This could be attributed to the slightly longer Si-O and Y-O bond lengths in O5 (see Table II). In $Y_2Si_3N_4O_3$, the spectra for O1, O2, and O3 show considerable differences in the shape of the broad peak. They are all fourfold coordinated, with bonds to one Si and three Y in O1 or two Si and two Y in O2 and O3. These differences can be related to the differences in the BLs (see Table II), especially the Si-O BL. The influence of the second NN effect such as the presence of N in these crystals cannot be ruled out either, although it is more difficult to quantify. In $Y_4Si_2O_7N_2$ or N-YAM, there are seven nonequivalent O sites. O1 through O5 have O-SiY3 coordination, and O6 and O7 have the O-Y4 coordination. They all have the double-peak structure in the first 7 eV range, but O6 and O7 have a lower edge onset. The differences in the edge onset contribute to the more broadened feature in the weight-averaged spectra in Fig. 1. The slight difference in the peak positions and shapes for the spectra of O atoms having the same coordination can again be correlated to the slight differences in their BLs, especially the Si-O BL. Figure 2 also shows that for O atoms having the same local coordination (O-SiY2, O-Si2Y2, O-SiY3, and O-Y4) in different crystals, their edge spectra need not be very close.

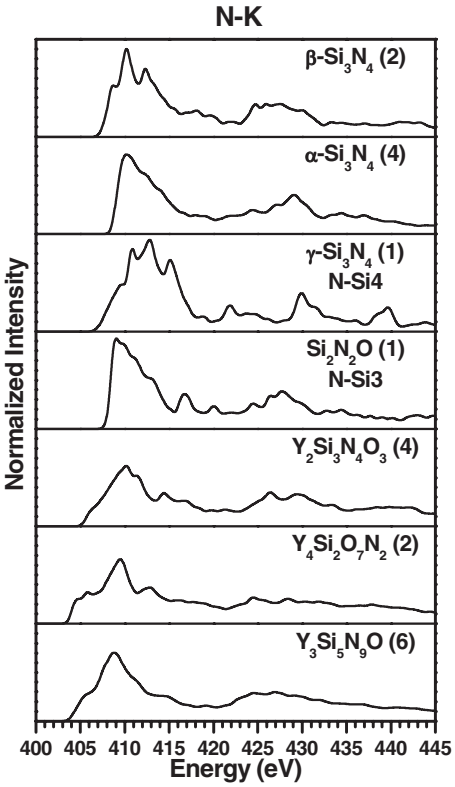

FIG. 3. Calculated total N-K edges in seven crystals. Notations are similar to Fig. 1.

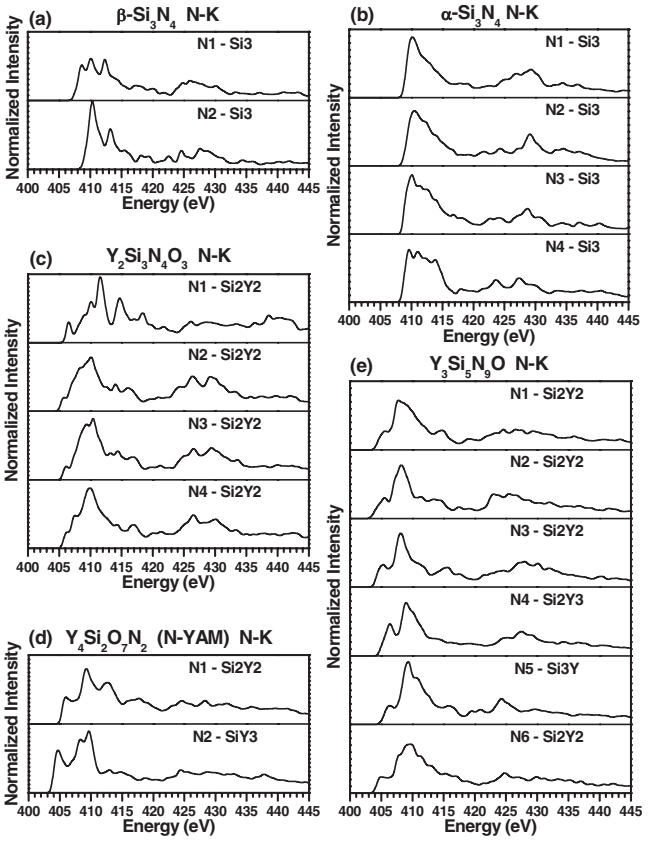

FIG. 4. The site-decomposed N-K edges in crystals with nonequivalent sites: (a) β-Si_3N_4, (b) $Y_2Si_3N_4O_3$, (c) $Y_4Si_2O_7N_2$, and (d) $Y_3Si_5N_9O$. The NN bonding coordination is indicated.

B. N-K edges

The calculated N-K edges for the seven N-containing crystals are displayed in Fig. 3. Of these seven crystals, only γ-Si_3N_4 and Si_2N_2O have a unique N site, and the huge difference between them is clearly due to their different local environments. N in γ-Si_3N_4 is fourfold bonded with one short bond to Si1 and three long bonds to Si2, whereas in Si_2N_2O, N has three nearly equal coplanar bonds. The N-K edge in γ-Si_3N_4 has multiple peaks, while in Si_2N_2O, the spectrum in the first 10 eV is an asymmetric peak with a steep edge onset. As with the O-K edges, the spectra for the nonequivalent N sites in the other five crystals (β-Si_3N_4, α-Si_3N_4, $Y_2Si_3N_4O_3$, $Y_4Si_2O_7N_2$, and $Y_3Si_5N_9O$) are displayed in Fig. 4, with their local coordination indicated. It can be seen that the N-K edges in these seven crystals are quite different even between β-Si_3N_4 and α-Si_3N_4, which are generally considered to be structurally similar except in the stacking sequences of the Si-N layers along the c axis. In β-Si_3N_4, there are two N sites (N1 and N2 in the ratio of 3 to 1); their K-edge spectra are very different. N1 has a three-peak structure, whereas N2 has a two-peak structure which lines up with peaks 2 and 3 in N1. The difference in the N-K edges from N1 and N2 in β-Si_3N_4 defies easy explanation. They both have planar bonding to three Si atoms and similar BLs. The only difference is that in N2, all three BLs are equal, while in N1, two of the three BLs are equal. Most likely, the second NN effect including the difference in bond angles (BAs) due to different layer stacking is at play. Indeed, the bond angles for N1 are 111.8°, 124.1°, and 124.1°, whereas the bond angles for N2 are all 120.0°, implying a perfect coplanar arrangement. However, it is still puzzling why the difference is so large. In α-Si_3N_4, there are four N sites in the ratio of 3:3:1:1. The differences between these four spectra are much less than the difference between N1 and N2 in β-Si_3N_4. Their weighted average, shown in Fig. 3, bears surprising resemblance to that of Si_2N_2O. However, it can still be recognized that the spectra of N3 and N4, which have all three Si-N BLs equal, are slightly different from those of N1 and N2, where all three Si-N BLs are different. We also note that N3 in α-Si_3N_4 has a perfect planar arrangement similar to N2 in β-Si_3N_4, yet their K edges are very different, underscoring the fact that BA effect alone cannot be used for a simple explanation. In $Y_2Si_3N_4O_3$, there are four N sites all having N-Si2Y2 coordination. Yet the spectrum for N1 is quite different from the other three, which are similar. Inspection of Table III reveals that the most likely cause is the shorter Si-N BL in N1 compared to the other three Ns. The $Y_4Si_2O_7N_2$ crystal has only two N sites of equal proportions. N1 bonds to two Si and two Y, and N2 bonds to one Si and two Y. Their spectra and absorption edges are very different. N1 has three peaks and N2 has only two peaks, with a smaller additional peak preceding the second peak. This difference signifies the importance of the NN atomic bonding to Si in the N-K edge. It is also noted that the single Si-N bond in N2 has a BL of 1.664 Å, considerably shorter than the two Si-N bonds of BL of 1.707 and

1.732 Å in N1. The N-rich $Y_3Si_5N_9O$ crystal has six different N sites with a weight factor of either 2 or 1 (see Table III). Four of them have Si2Y2 coordination (N1, N2, N3, and N6), one with N-Si2Y3 coordination (N4), and the other has N-Si3Y coordination (N5). Their spectra differ, but not as dramatically as in $Y_4Si_2O_7N_2$. In this crystal, the Si-N BLs are much longer than those in other N-containing crystals and this could be the reason for the smaller deviations of their K-edge spectra. We have also noted that the weight-averaged N-K edges in $Y_2Si_3N_4O_3$ and $Y_3Si_5N_9O$ show sufficient similarity, underscoring the difficulty to distinguish them experimentally.

C. Si-K and Si-L edges

The Si-K and Si-L edges in many inorganic and mineral crystals have been intensively investigated both experimentally and theoretically.[73–80] The Si-K edges from 11 crystals are presented in Fig. 5. Six of these crystals have unique Si sites and five of them have multiple Si sites. The site-specific spectra in these five crystals are presented in Fig. 6. Si always has a fourfold tetrahedral coordination with well-defined NN coordination. Under high pressure, Si can assume octahedral coordination with O (as in stishovite) and N (as in γ-Si_3N_4). The spectacular differences in the Si-K edges, especially in the first 5–10 eV, present a real challenge for interpretation. We first focus on those crystals with unique Si sites. The difference in Si-K edges between α-SiO_2 and stishovite has been discussed in many past calculations,[19,31,73–76,80] and is due primarily to the different NN numbers of 4 and 6, respectively. Both have a strong leading peak, which is much sharper in α-SiO_2 than in stishovite. Stishovite has a secondary peak at a slightly higher energy, which gradually decreases its intensity in the energy range at least 5 eV above it. The interesting point is to compare the Si-K edge in α-SiO_2 with that of $Y_2Si_2O_7$ and Y_2SiO_5; all have the same Si-O4 local coordination. The spectrum for α-SiO_2 is a single sharp peak, but that of $Y_2Si_2O_7$ is a broader double peak and that of Y_2SiO_5 is a very broad plateaulike peak. The BLs of these four Si-O bonds are not drastically different (see Table IV), so the only logical explanation for these observed differences must come from the NNN effect or the bond angle effect. In α-SiO_2, Si has four NNN Si atoms at the separation of 3.059 Å. In $Y_2Si_2O_7$ (Y_2SiO_5), it has only one Y as a NNN with a distance of separation of 3.135 Å (3.106 Å). Since Y is a much larger ion than Si and its wave function extends further than Si, reasonable interaction between Si and Y can be expected. Nonetheless, this still cannot explain the differences between the Si-K edges in the two ternary yttrium silicates. A possible explanation is that two of the Si-O bonds in Y_2SiO_5 are relatively shorter (1.602 and 1.605 Å) than in the other two crystals. Furthermore, Si in Y_2SiO_5 has a NNN Y at a distance of 3.106 Å, whereas for Si in $Y_2Si_2O_7$, the distance to the NNN Y is a littler farther (3.135 Å). This clearly illustrates that the finger printing argument fails in complex crystals even in the most favorable case of tetrahedral Si-O4. We next compare the Si-K edges in β-Si_3N_4 with Si-N4 coordination and in Si_2N_2O with the Si-ON3 coordination. Interestingly, in these cases, the Si-K edges are also dominated by a leading peak, like Si in α-SiO_2 with Si-O4 coordination. The Si-K edge in Si_2N_2O is only marginally different from that in α-SiO_2. The Si-K edge in β-Si_3N_4 has a more broadened peak with additional structures in the higher energy range. It appears that the effect of having N or O as a NN to Si on Si-K edge is not a drastic one, but a gradual one. Thus, a simple finger printing argument cannot distinguish these two cases. We will further discuss this point in Sec. V.

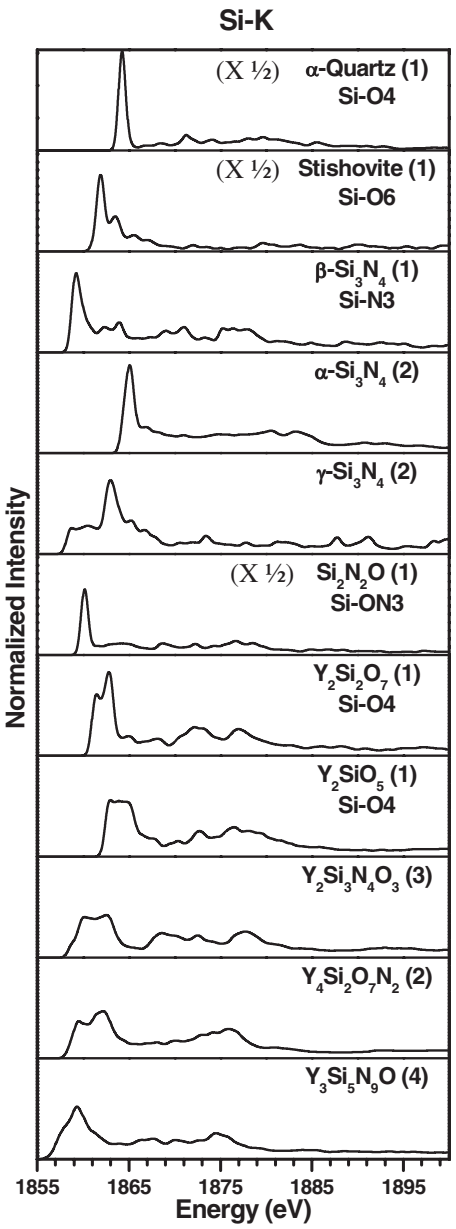

FIG. 5. Calculated Si-K edges in nine crystals. The notations are similar to Fig. 1. In α-SiO_2 and stishovite, the spectra are scaled with a factor of 1/2.

We now turn to the spectra shown in Fig. 6 for crystals with multiple Si sites. α-Si_3N_4 has two Si sites with almost identical local environments. So the fact that Si2 has a much sharper leading peak than Si1 is somewhat difficult to explain. This is similar to the case of the N-K edges in α-Si_3N_4

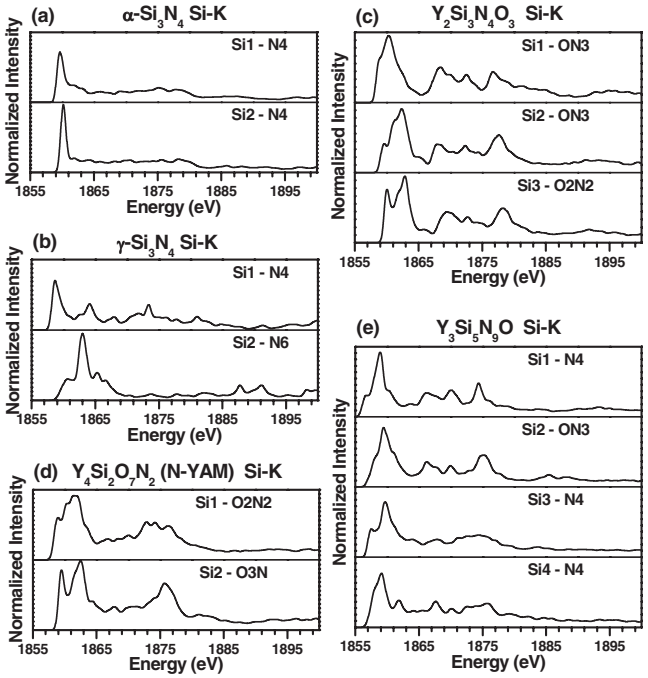

FIG. 6. The site-specific Si-K edges in crystals with nonequivalent sites: (a) $Y_2Si_3N_4O_3$, (b) $Y_4Si_2O_7N_2$, and (c) $Y_3Si_5N_9O$. The NN bonding coordination is indicated.

discussed above, and could be related to the NNN effect. The difference in the Si-K edges between Si1 (tetrahedral site) and Si2 (octahedral site) in γ-Si_3N_4 is the most dramatic one, and neither of them resembles the spectrum of the weighted sum shown in Fig. 5. This has already been discussed in the previously published work.[15,32] Obviously, the number of NNs (4 vs 6) and their BLs play an important part. The difference in the Si-K edges of Si1 and Si2 in γ-Si_3N_4 is much larger than the differences between Si-O4 (in α-SiO_2) and Si-O6 (in stishovite). This again underscores the point that for calculated spectra to be comparable with the measured ones in crystals where nonequivalent sites exist, a weighted sum of the individual spectra must be used. The Si-K edges in the three quaternary crystals have a variety of local coordinations including Si-ON3 (Si1 and Si2 in $Y_2Si_3N_4O_3$, and Si2 in $Y_3Si_5N_9O$), Si-O2N2 [Si3 in $Y_2Si_3N_4O_3$, Si1 in $Y_4Si_2O_7N_2$ (N-YAM)], Si-O3N (Si2 in N-YAM), and Si-N4 (Si1, Si2, and Si4 in $Y_3Si_5N_9O$). The Si-K edge for Si_2N_2O which has a Si-ON3 configuration has a much sharper leading peak than Si1 and Si2 in $Y_2Si_3N_4O_3$. This enables us to ascertain if there is a systematic change when the four NNs of Si are gradually changed from having four O to four N as NNs. This will be discussed later in Sec. V. However, it should be pointed out that there are noticeable differences between the Si-K edges of the same configurations in the same crystal such as Si1 and Si2 in $Y_2Si_3N_4O_3$, or in different crystals (Si2 in $Y_3Si_5N_9O$). These differences may be partially explained by the differences in their BLs as listed in Table IV. The other observations from Fig. 6 are the following: (1) In $Y_2Si_3N_4O_3$, the spectra from the three Si ions show differences in the first 6 eV range. Si1 has a single peak and a shoulder, Si2 has a single peak and two shoulders,

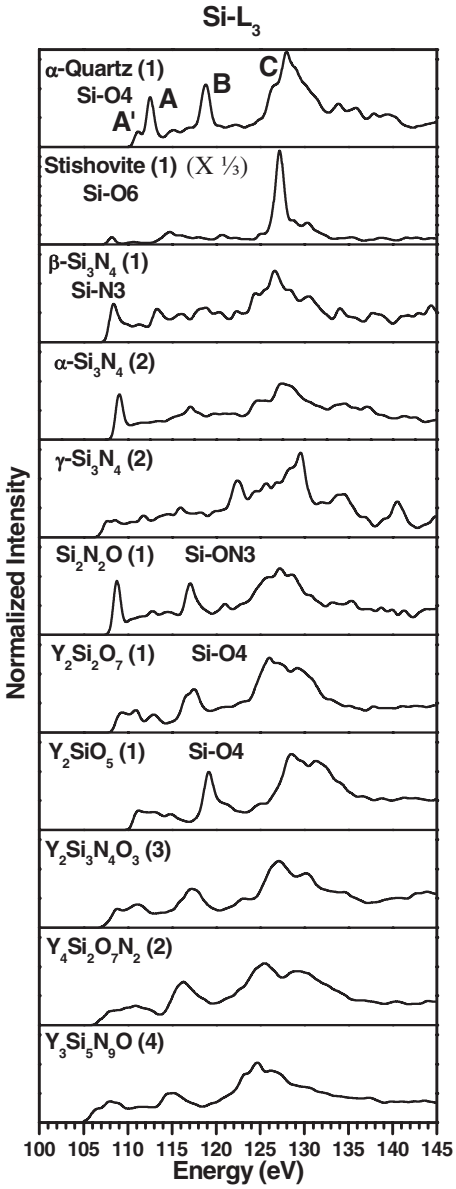

FIG. 7. Calculated Si-L_3 edges in nine crystals. The labeling is similar to Fig. 5.

and Si3 has two peaks. (2) In $Y_4Si_2O_7N_2$, the two Si atoms have very different spectra. Si1 with O2N2 coordination has a broad peak with some shoulderlike structures, and Si2 with O3N coordination has two sharp peaks. (3) In $Y_3Si_5N_9O$, the four Si-K spectra show similar patterns, but with discernable differences in peak structures, mainly in the first 8 eV range.

We now come to discuss the results of the Si-L_3 edge in the same 11 crystals which are presented in Fig. 7. This is followed by the site-specific L_3 edges for crystals with nonequivalent Si sites in Fig. 8. The L_3 edge, which basically probes the $(s+d)$ type of states in the CB, is very different from the K edge. In Si, the transition energy of the $2p$ core electron to the CB is much less than the transition energy from the $1s$ core electron. Hence, some of the observations described above for the Si-K edges do not necessarily hold true for the Si-L_3 edges. Still, there are some similarities in

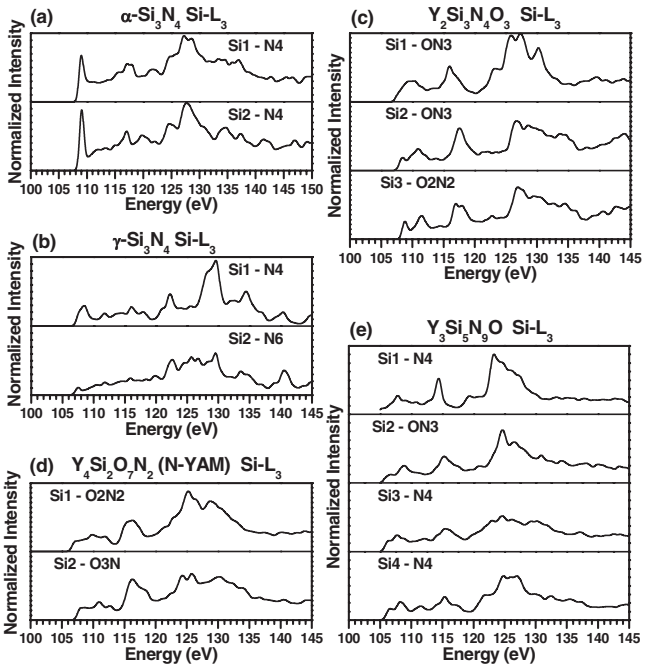

FIG. 8. The site-specific Si-L_3 edges in crystals with nonequivalent sites: (a) $Y_2Si_3N_4O_3$, (b) $Y_4Si_2O_7N_2$, and (c) $Y_3Si_5N_9O$. The labeling is similar to Fig. 6.

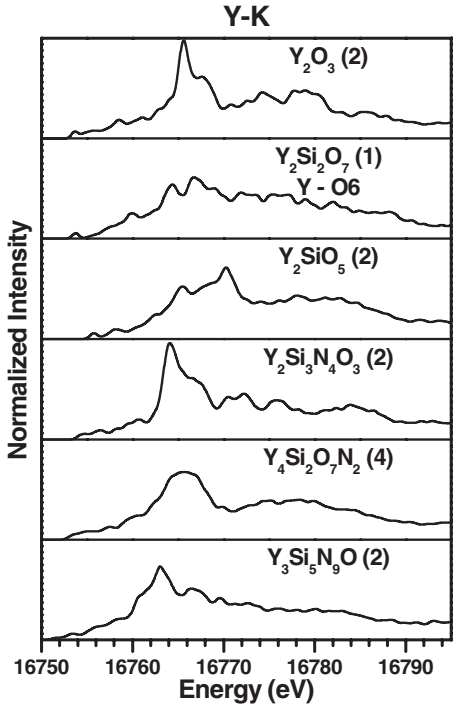

FIG. 9. Calculated total Y-K edges in six crystals. The notations are similar to Fig. 1.

the overall characterization. From Figs. 7 and 8, we briefly summarize our observations as follows, along the line discussed for the Si-K edges. (1) In Fig. 7, the Si-L_3 edge in α-SiO_2 shows three well-defined peak structures *A*, *B*, and *C* over a diffuse background. *A* is preceded by a weaker peak *A′* near the absorption edge, *B* is about 6.37 eV above *A*, and *C* is broader, with the peak centered at 9.35 eV above *B*. (2) In stishovite, peak *C* becomes overwhelmingly dominating and shifts slightly to a lower energy. Peaks *A* and *B* are barely visible. This huge difference between the fourfold Si in α-SiO_2 and sixfold Si in stishovite is more dramatic than in the Si-K edges. (3) The single site Si ions in $Y_2Si_2O_7$ and Y_2SiO_5 both have Si-O4 coordination, and their L_3 edges are quite similar. They show some resemblance to the spectrum in α-SiO_2 except that the three peaks are more broadened, especially for peaks *A* which are flatter. These can be related to the differences in BLs and also the possible NNN effects. (4) By comparing Si-L_3 edges in binary nitrides (β-Si_3N_4 and α-Si_3N_4) that have Si-N4 coordination to the Si-O4 coordination in α-SiO_2, the differences are quite remarkable. In β-Si_3N_4, peak *A* moved down toward the absorption edge, peak *C* becomes even more broadened, and peak *B* disappeared or transformed into multiple ripplelike features. These differences are much larger than those found in the Si-K edges. (5) The Si-L_3 edge spectrum in Si_2N_2O (a single Si site with coordination of Si-ON3) lies somewhere between that of α-SiO_2 with Si-O4 coordination and that of β-Si_3N_4 with Si-N4 coordination. This is the strongest case so far that shows a spectral correlation to the chemical species of the NN atoms. We will return to this point later in Sec. V. (6) The weight-averaged spectrum for Si-L_3 in α-Si_3N_4 is close to that for β-Si_3N_4, but they are drastically different from that for γ-Si_3N_4 since the two Si sites in the latter are very different (fourfold and sixfold with very different BLs). As can be seen in Fig. 8(b), the spectrum for the tetrahedral Si (Si1) has more peaks in the first 25 eV range, while that of octahedral Si (Si2) is almost featureless in the first 15 eV range. (7) The weight-averaged Si-L_3 spectra in the three quaternary crystals show surprisingly similar features. In $Y_2Si_3N_4O_3$, we can divide the spectral range into three regions: (a) the first 6 eV from edge onset, (b) the next 10 eV, and (c) those above 125 eV. The three Si-L_3 spectra show some differences in region (a), minor differences in region (b), and considerable differences in region (c) in their shapes and peak positions. In $Y_4Si_2O_7N_2$, the two Si-L_3 edges (with Si-O2N2 and Si-O3N coordinations) show much less deviation than in Si-K edges of Fig. 6(d). In $Y_3Si_5N_9O$, the four Si edges show some differences in the three regions defined above, especially for Si1 which has a much sharper peak in region (b) and a highly asymmetric but broader peak in region (c).

D. Y-K and Y-L_3 edges

The ELNES/XANES spectra of Y in inorganic crystals are much less commonly reported in the literature. Experimentally, it requires a much higher energy source to excite the deep core electrons from a heavy element such as Y, especially for the Y-K edge. Modern synchrotron facilities do have this capability, but the spectra obtained are usually of poor energy resolution. Here, theoretical calculations can provide a useful complement to such measurements. The calculated Y-K edges in the six crystals are presented in Fig. 9, which show large variations in terms of their peak positions and shapes. Of these six crystals, only $Y_2Si_2O_7$ has a unique

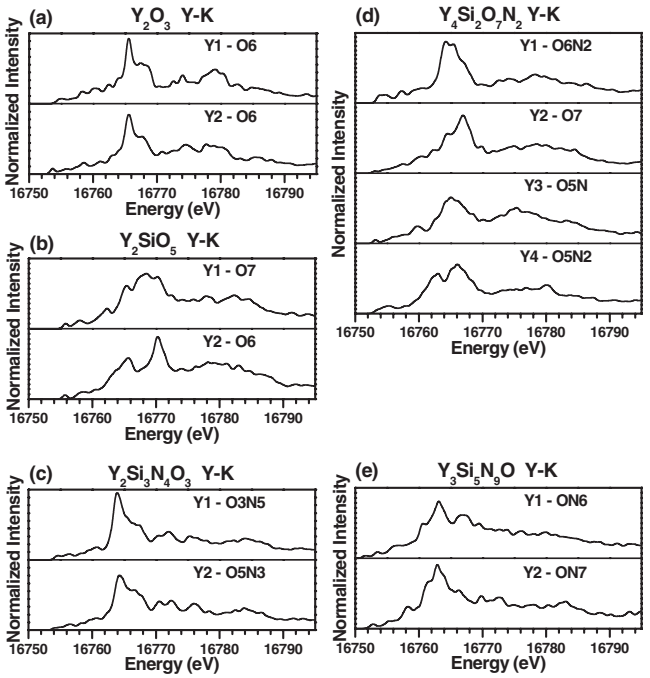

FIG. 10. The site-specific Y-K edge in crystals with nonequivalent sites: (a) Y_2O_3, (b) Y_2SiO_5, (c) $Y_2Si_3N_4O_3$, (d) $Y_4Si_2O_7N_2$, and (e) $Y_3Si_5N_9O$. The NN bonding coordination is indicated.

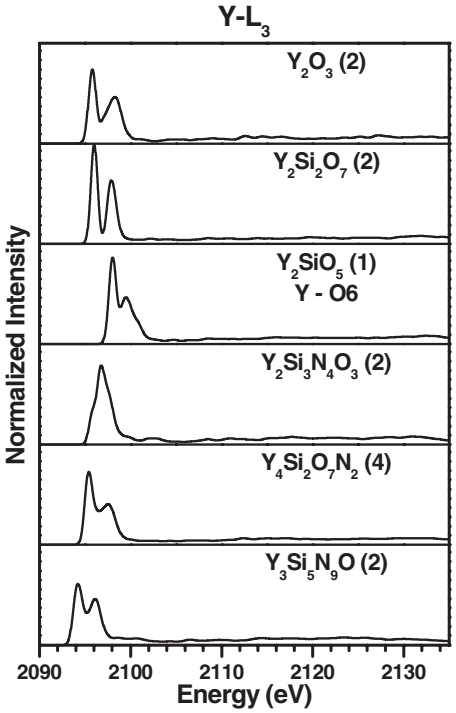

FIG. 11. Calculated total Y-L_3 edges in six crystals. The labeling is the same as in Fig. 9.

Y site with Y-O6 coordination, but actually shows the least distinguished features. Figure 10 shows the Y-K spectra for the five crystals with different Y sites and their coordination. Table V indicates that Y atoms in these crystals can have six-, seven-, and eight-fold coordinations to different numbers of O and N atoms, with Y-O6 being the most common one. One would, thus, expect the Y-K edges in $Y_2Si_2O_7$ and Y_2O_3 as well as Y2 in Y_2SiO_5 to be somewhat close to each other. This is not the case. Y_2O_3 has two Y sites both having Y-O6 coordination and their spectra are very close, but not with the spectra from the other two crystals with the same coordination. The most logical explanation to this unexpected variation is the presence of Si in $Y_2Si_2O_7$ and Y_2SiO_5, or the NNN effect, since there are no large differences in their BLs (see Table V). The difference between the Y spectrum in $Y_2Si_2O_7$ and the spectra from the two Y sites in Y_2SiO_5 is more difficult to explain. In Y_2SiO_5, the K edge for Y1 is almost featureless with a rather broad peak, while the spectrum for Y2 has a well resolved two-peak structure. On the other hand, there is a much closer resemblance between the Y-K edges in Y_2O_3 and $Y_2Si_3N_4O_3$. The two Y sites, Y1 and Y2, in $Y_2Si_3N_4O_3$ have local coordinations of Y1-O3N5 and Y2-O5N3, respectively, they are eightfold bonded, and with different numbers of N atoms as NNs. In the $Y_4Si_2O_7N_2$ crystal, there are four Y sites with different coordinations of Y1-O6N2, Y2-O7, Y3-O5N, and Y4-O5N2, respectively, and their spectra show considerable differences in the shapes and positions of the main broad peak. In the $Y_3Si_5N_9O$ crystal, the two Y sites with coordinations of ON6 and ON7 have similar spectra. On the other hand, the spectrum for Y1 in Y_2SiO_5 and for Y2 in $Y_4Si_2O_7N_2$ both have a Y-O7 configuration and show a marked difference. All these indicate that at least in the case of Y-K edges, there is no clear evidence of any correlations in the spectra to their local NN environments.

The Y-L_3 spectra for the six crystals are presented in Fig. 11. The site-specific spectra for five of these crystals having nonequivalent sites are shown in Fig. 12. The weight-averaged Y-L_3 edges in Fig. 11 show mostly a double-peak structure of varying intensity ratios and different separations between the two peaks except for Y-L_3 in $Y_2Si_3N_4O_3$, where there is only a single peak. In Y_2SiO_5, the L_3 edges of Y1 and Y2 with coordinations of Y1-O7 and Y2-O6 show variations due to the extra O as a NN to Y1. There are two Y sites in $Y_2Si_3N_4O_3$ with coordinations of Y-O3N5 and Y-O5N3, respectively, but they both have a single-peak structure. This is similar to the Y-K edges for these two sites discussed above. The other cases with a single peak in the Y-L_3 spectrum occurs in Y4 of $Y_4Si_2O_7N_2$ (coordination Y-O5N2), and in Y2 of $Y_3Si_6N_9O$ (coordination Y-ON7). Y1 in $Y_4Si_2O_7N_2$ having a coordination of Y-O6N2 actually has a plateaulike structure. The Y sites having O6 coordination (Y1, Y2 in Y_2O_3 and Y2 in Y_2SiO_5) show similar two-peak structure and intensity ratios. The only discernable difference appears to be that in Y_2SiO_5, the separation of the two peaks is much less, about 0.7 eV, and the absorption edge is at a higher energy. The other cases that have a distinct two-peak structure in the L_3 edge are Y2 and Y3 in $Y_4Si_2O_7N_2$ (coordination Y-O7 and Y-O5N) and Y1 in $Y_3Si_6N_9O$ (coordination Y-ON6). The Y1 site in Y_2SiO_5 with the same coordination of Y-O7 as Y2 in $Y_4Si_2O_7N_2$ has two peaks that are much closer and which have less intensity variations.

The above analysis of the L_3 edges in the six Y-containing crystals shows that there is no clear correlation between the

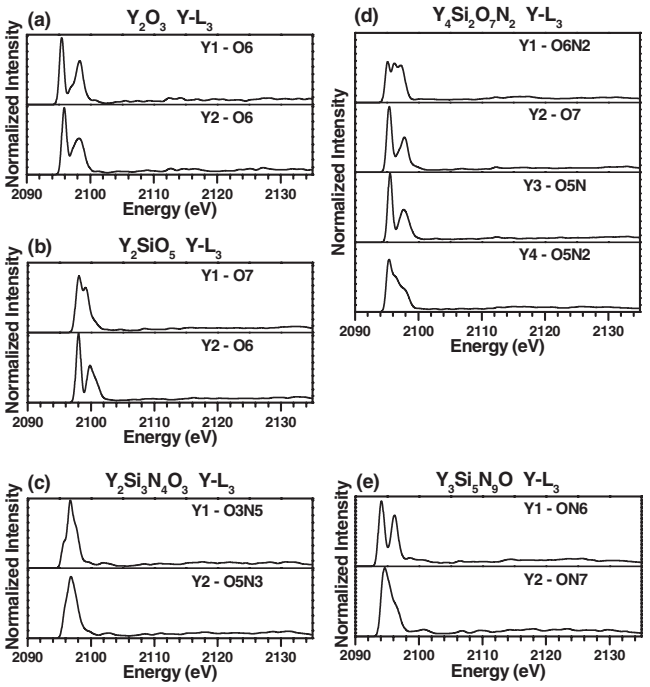

FIG. 12. The site-specific Y-L_3 edge in crystals with nonequivalent sites: (a) Y_2O_3, (b) Y_2SiO_5, (c) $Y_2Si_3N_4O_3$, (d) $Y_4Si_2O_7N_2$, and (e) $Y_3Si_5N_9O$. The labeling are the same as in Fig. 10.

peak structures of the spectra and the NN coordination of the Y ions, more so than for the Y-K edges. Why this is the case is not all clear. One possible reason is that the states with *s* or *d* symmetries in the CB for the Y-containing crystals are much more spread out. The variations of their spectra due to interactions at larger distances and the subsequent changes in the electronic structure cannot be easily quantified.

V. DISCUSSIONS

The data presented in Sec. IV are overwhelming and, to a large extent, fail to provide a clear picture regarding the possibility of finding a correlation between the calculated spectra and the local atomic-scale environment of the ions in Y-Si-O-N crystals. It is necessary to sift through the data in an organized fashion to seek any potential correlations such that key questions can be answered simply by yes or no. Specifically, we will answer the following five questions by recapturing the special features from the large amount of spectral data of anions (O, N) and cations (Si, Y) presented above.

(1) Are there any spectral features in the calculated spectra that can be clearly correlated with the number of NN atoms?

(2) For a given number of NN atoms, are there any correlations or trends in the spectral features with the atomic species of the NN atoms?

(3) Is there any strong evidence in (1) and (2) that the changes in the spectral features can be accounted for by variations in the BLs?

(4) Is there any evidence in (1) and (2) for the NNN effect in the correlations or trends in (1) and (2)?

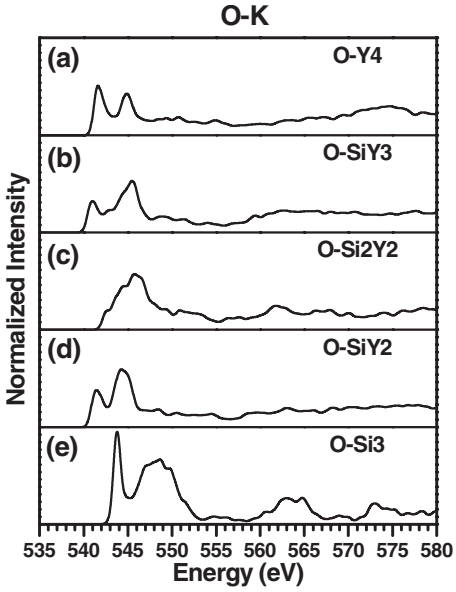

FIG. 13. O-K edges with similar nearest neighbor coordination: (a) O-Y4 from O1 in Y_2SiO_5, (b) O-SiY3 from O2 in $Y_4Si_2O_7N_2$, (c) O-Si2Y2 from O1 in $Y_2Si_3N_4O_3$, (d) O-Si-Y2 from O2 in $Y_2Si_2O_7$, and (e) O-Si3 from stishovite.

(5) Is there any specific difference in the above observations between cations and anions in general? between anions O and N? and between cations Si and Y?

The answer to question (1) is clearly no. O has coordination numbers of 2, 3, and 4, and N has coordination numbers of 3, 4, and 5. From Figs. 1 and 3, the O-K and N-K edges are very different for different numbers of NN, and no systematic trend can be observed. Si always has four NN atoms, except for Si2 in γ-Si_3N_4 which has six. We have already pointed out in Sec. V C that Si in α-SiO_2, $Y_2Si_2O_7$, and Y_2SiO_5 all have four O as NNs, but their spectra differ completely. There are only two cases for Si with six NN (Si-O6 in stishovite and Si-N6 for Si2 in γ-Si_3N_4). The complete difference in the spectra of these two high pressure phases has already been commented upon. Y has NN numbers of 6, 7, and 8. From Figs. 9 and 10, no specific features of any kind can be identified in either the Y-K or the Y-L spectra. This lack of correlation in the spectra with the number of NN atoms for both anions and cations is related to questions (2)–(4).

The answer to question (2) is a weak yes, with some exceptions which are related to questions (3) and (4). This is illustrated in Figs. 13(a)–13(c) for O with four NN, where the O-K edges of configurations O-Y4, O-SiY3, and O-Si2Y2 are shown. There is a clear trend in going from a configuration of O-Y4 to O-SiY3 and then to O-Si2Y2. The two-peak structure in Fig. 13(a) changes to a one-peak structure in Fig. 13(c) with concomitant changes in the intensity and broadening. There are only two cases of O with a three NN coordination number, O-SiY2 in $Y_2Si_2O_7$ and Y_2SiO_5, and O-Si3 in stishovite, so we cannot speak of any trends. Their spectra are very different [see Figs. 13(d) and 13(e)]. In stishovite, the spectrum consists of a sharp leading peak, and a broad second peak whereas in the two ternary silicates

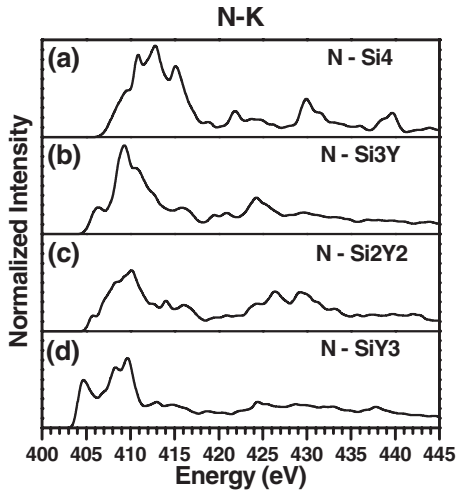

FIG. 14. N-K edges with a nearest neighbor coordination number of 4: (a) N-Si4 from γ-Si_3N_4, (b) N-Si3Y from N5 in $Y_3Si_5N_9O$, (c) N-Si2Y2 from N2 in $Y_2Si_3N_4O_3$, and (d) N-SiY3 from N2 in $Y_4Si_2O_7N_2$.

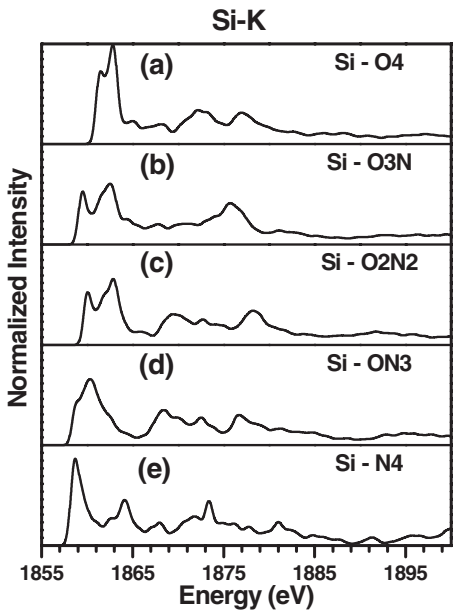

FIG. 15. Si-K edges with a nearest neighbor coordination number of 4: (a) Si-O4 in Si in $Y_2Si_2O_7$, (b) Si-O3N from Si2 in $Y_4Si_2O_7N_2$, (c) Si-O2N2 from Si3 in $Y_2Si_3N_4O_3$, (d) Si-ON3 from Si1 in $Y_2Si_3N_4O_3$, and (e) Si-N4 from Si1 in γ-Si_3N_4.

with two Y ions in the NN shell, the second peak is well defined and relatively sharp and its position is close to the first sharp peak in O-Si3 of Fig. 13(e). In the case of N with coordination numbers 3 (all to Si) and 4 (to Si and Y), we can only discuss the second case. The answer is again a weak yes with exceptions. Figure 14 shows the spectra from selected crystals with configurations of N-Si4, N-Si3Y, N-Si2Y2, and N-SiY3 in increasing order of the number of NN Y ions. There is a general trend. The absorption edge decreases as the number of Si in the NN shell decreases. There is also a shift in the spectral weight toward lower energy as the number of multiple peaks changes from 3 to 2 to 1, and then back to 2 in going from Fig. 14(a) to Fig. 14(d).

The most definitive "yes" answer for question (2) is for Si with four NN atoms, the most common tetrahedral configuration in all silicates. In Fig. 15, we show the Si-K edges with different numbers of O/N ratios: (a) Si-O4, (b) Si-O3N, (c) Si-O2N2, (d) Si-ON3, and (e) Si-N4. We selected these spectra from the more complex crystals instead of the ones with simpler structures (α-SiO_2 and Si_2N_2O) since they are more representative of complex systems. The change in the spectra as the O/N ratio changes is very clear. First, the absorption edge shifts to lower energy in going from (a) to (e). From (a) to (b) and (c), the double peak changes their relative intensity and peak separations. The change from (b) to (c) is smaller in the first 10 eV range, but more obvious in the range above the first 10 eV. In going from (c) to (d), the double peak evolves into a broader single peak with a shoulder, but less change in the structures above 10 eV. Finally, the Si-N4 configuration in (e) shows a sharp peak near the absorption edge and more structures in the range 5 eV above the edge. On the other hand, the answer to question (2) for Y edges is "no" because the spectral variations for a given number of NN are quite complex and they are very much influenced by the answers to questions (3) and (4) below.

The answer to question (3) is yes in most cases. As discussed in the previous sections, there are cases where the discrepancy in the spectra can be best explained as due to the possible variations in the BLs. The NN BL controls the specific interatomic interaction and affects their electronic structure in the CB to a large extent. Unfortunately, in multicomponent complex crystals, the effect due to variations in the BL cannot be quantified and can only be discussed in the general context of the maximum and the minimum BLs for a given configuration as listed in Table V.

The answer to question (4) is similar to question (3), but is even less definitive. From the results of the previous section, it is obvious that the second NN can play an important role, especially in multicomponent crystals. For example, the presence of Y as a NNN to Si can apparently explain the difference in the Si-K and Si-L edges of the ternary and quaternary crystals. Unfortunately, the second NN effect is also very difficult to quantify. Further, we did not investigate the BA variations with the spectral features. We feel that such endeavor would be fruitless since any spectral correlation, even if they exist, would be weak, not definitive. What we are looking for is already very complicated just based on the NN environments. It may be feasible that in simpler and more specific systems, such as in the case of passive defects in crystalline Si,[35] variations with BA could be attempted to gain further insight. Here, our conclusions with the NNN effect is mostly inferred from the presence of the NNN ions, especially the larger and more ionic Y ions.

The answer to question (5) is necessarily general in nature, but is quite important. Obviously, there are differences between cations (Si,Y) and anions (O,N) in our discussions. This is because the cations in these crystals have more of their PDOS in the CB region due to the charge transfer to anions, while anions have more PDOS in the VB region.[27,28] One would then expect that it would be easier to seek corre-

lations in the ELNES/XANES spectra in cations rather than anions. This is generally not true. Although a clear trend can be established for Si with four NN atoms, it is certainly not for Y. The differences between Si and Y can be many. The most important one is the ionicity, which affects the charge transfer and the presence of the 4*d* electrons in Y. Y is also a larger ion with larger interatomic BLs and can bond to more atoms but with weaker bonds. This has been illustrated in many of our past calculations of the electronic structures of Y-containing crystals.[24–29,81,82] The difference between O and N is less dramatic than the difference between Si and Y. Still we can see there are marked variations in their trends. Again, this can be attributed to the ionicity of O and N. They have formal charges of −2 and −3, respectively, which can certainly affect their electronic structure and bonding in a very significant way. Another important issue is for the $L_{2,3}$ edges of the transition metal ions; it may need to use the more complicated multiplet theory[51,83,84] for proper interpretation, which is beyond the scope of the present paper.

A few additional comments related to the above discussions may be in order. First, we have mentioned the differences in the edge onset of various spectra obtained as the difference in the calculated total energies of the initial and final states. We cannot rule out the numerical inaccuracy associated with different sizes of the supercells for different crystals (see Table I). However, the edge onset for different sites in the same crystal using the same supercell should be accurate. We have also not considered the anisotropy of the spectra for noncubic crystals, which could result in additional complexity.[18] Since it is not our intention in this paper to compare with any experimental measurements, we feel it is better to focus on the directionally averaged spectra for our discussion. In more focused studies limited to a few crystals, anisotropic effect can be studied using the same method and approach. The present calculations are at the level of density functional theory with a further step to account for the electron core-hole interaction. More elaborate many-body corrections beyond DFT is clearly impractical for complex ceramics at this stage.

VI. CONCLUSIONS

Based on the *ab initio* calculations of the ELNES/XANES spectra (O-K, N-K, Si-K, Si-L_3, Y-K, and Y-L_3 edges) of the anions (O, N) and cations (Si,Y) in 12 crystals of the Y-Si-O-N system, attempts were made to correlate the calculated spectra with the local structural environments of each atom. We found that, with the exception of the fourfold coordinated Si ion, there is no clear correlation that can qualify for the much discussed and celebrated finger printing capability of the ELNES/XANES spectra. For the O-K and N-K edges, there are many counterexamples to the perceived correlations that can be traced to effects beyond the NN or to variations in BLs and BAs. In the Y-K and Y-L_3 edges, no meaningful correlations can be established. For simpler crystals where nonequivalent sites of a particular ion exist, the weighted sum of the spectra from individual sites must be used for comparison with experiment. These results indicate that for proper interpretation of the experimentally measured spectra in complex ceramics, or ceramic materials containing microstructures, theoretically calculated spectra from simple crystals with similar coordination will not be useful. For complex systems, the spectral features cannot be predicted by a simple scheme or schemes. Attempts to model the measured spectra with a series of Gaussian peaks centered at different energies and explain the spectral features with reference to the peaks in simple crystals is a fruitless endeavor. In nanostructured materials, or materials containing defects, impurities, grain boundaries, or at the interfaces with other dissimilar crystals, no broadly applicable and quantitative methods are available.[85] It is our opinion that a more promising approach is to carry out detailed structural modeling followed by accurate electronic structure and spectral calculations. This is necessary because the subtle changes in the electronic structure in structurally complicated materials as a result of structural changes beyond the nearest neighbors, especially in the CB region, cannot be simply inferred from those of the simple crystals. The correctness of the structure of a particular system such as in grain boundaries or interfaces can be judged by comparing the calculated spectra of different structural models with the experimental measurements. Future development of ELNES/XANES computational capabilities should focus on an improvement to the speed of computation and the efficiency with which such data can be analyzed. The present work clearly demonstrates the power and utility of accurate *ab initio* spectral calculations. The theoretically calculated spectra can serve as a useful guide in the characterization of complex materials systems, especially when the experimental measurements are unlikely to match the resolution and the site specificity of the calculations.

ACKNOWLEDGMENTS

Work is supported by the U.S. Department of Energy under Grant No. DE-FG02-84DR45170. This research used the resources of NERSC supported by the Office of Science of the U. S. DOE under Contract No. DE-AC03-76SF00098. This research was partially supported by NSF Grant No. DMR-00162 in collaboration with NANOAM Project of EUCODIS (G5RD-CT-2001-00586) in the early stage of the work.

*Corresponding author: chingw@umkc.edu

[1] R. F. Egerton, *Electron-energy Loss Spectroscopy in the Electron Microscope* (Plenum, New York, 1996), Chap. 5.

[2] D. A. Muller, T. Sorsch, S. Moccio, F. H. Baumann, K. Evans-Luuerodt, and G. Timp, Nature (London) **399**, 758 (1999).

[3] D. Vlachos, A. J. Craven, and D. W. McComb, J. Phys.: Condens. Matter **13**, 10799 (2001).

[4] M. Malvestuto, R. Carboni, F. Boscherini, F. D'Acapito, S. Spiga,

M. Fanciulli, A. Dimoulas, G. Vellianitis, and G. Mavrou, Phys. Rev. B **71**, 075318 (2005).
[5] M. Bosman, M. Watanabe, D. T. L. Alexander, and V. J. Keast, Ultramicroscopy **106**, 1024 (2006).
[6] R. F. Egerton, Micron **34**, 127 (2003).
[7] V. J. Keast and M. Bosman, Microsc. Res. Tech. **70**, 211 (2007).
[8] D. A. Muller, Y. Tzou, R. Raj, and J. Silcox, Nature (London) **366**, 725 (1993).
[9] F. W. Lytle, R. B. Greegor, and A. J. Panson, Phys. Rev. B **37**, 1550 (1988).
[10] L. A. J. Garvie, A. J. Craven, J. Alan, and R. Brydson, Am. Mineral. **80**, 1132 (1995).
[11] F. Farges and G. Brown, Jr., Geochim. Cosmochim. Acta **61**, 1863 (1997).
[12] M. E. Fleet and S. Muthupari, J. Non-Cryst. Solids **255**, 233 (1999).
[13] Z. Wu, C. Romano, A. Marcelli, A. Mottana, G. Cibin, G. Della Ventura, G. Giuli, P. Courtial, and D. B. Dingwell, Phys. Rev. B **60**, 9216 (1999).
[14] A. N. Mansour, A. Marcelli, G. Gibin, G. Yalovega, T. Sevastyanova, and A. V. Soldatov, Phys. Rev. B **65**, 134207 (2002).
[15] I. Tanaka, T. Mizoguchi, T. Sekine, H. He, K. Kimoto, S.-D. Mo, and W. Y. Ching, Appl. Phys. Lett. **78**, 2134 (2001).
[16] Y.-N. Xu, Y. Chen, S. D. Mo, and W. Y. Ching, Phys. Rev. B **65**, 235105 (2002).
[17] T. Mizoguchi, I. Tanaka, M. Kunisu, M. Yoshiya, H. Adachi, and W. Y. Ching, Micron **34**, 249 (2003).
[18] T. Mizoguchi, I. Tanaka, S. Yoshioka, M. Kunisu, T. Yamamoto, and W. Y. Ching, Phys. Rev. B **70**, 045103 (2004).
[19] W. Y. Ching, L. Ouyang, P. Rulis, and I. Tanaka, Phys. Status Solidi B **242**, R94 (2005).
[20] W. Y. Ching and P. Rulis, Phys. Rev. B **73**, 045202 (2006).
[21] Y. Sato, T. Mizoguchi, F. Oba, M. Yodogawa, T. Yamamoto, and Y. Ikuhara, Appl. Phys. Lett. **84**, 5311 (2005).
[22] T. Mizoguchi, Y. Sato, J. P. Buban, K. Matsunaga, T. Yamamoto, and Y. Ikuhara, Appl. Phys. Lett. **87**, 241920 (2005).
[23] T. Mizoguchi, A. Seko, M. Yoshiya, H. Yoshida, T. Yoshida, W. Y. Ching, and I. Tanaka, Phys. Rev. B **76**, 195125 (2007).
[24] W. Y. Ching, Yong-Nian Xu, and L. Ouyang, J. Am. Ceram. Soc. **86**, 1410 (2003).
[25] W. Y. Ching, L. Ouyang, and Y.-N. Xu, Phys. Rev. B **67**, 245108 (2003).
[26] L. Ouyang, H. Yao, S. Richey, Y.-N. Xu, and W. Y. Ching, Phys. Rev. B **69**, 094112 (2004).
[27] W. Y. Ching, L. Ouyang, H. Yao, and Y. N. Xu, Phys. Rev. B **70**, 085105 (2004).
[28] W. Y. Ching, J. Am. Ceram. Soc. **87**, 1996 (2004).
[29] Y.-N. Xu, P. Rulis, and W. Y. Ching, Phys. Rev. B **72**, 113101 (2005).
[30] S. D. Mo and W. Y. Ching, Phys. Rev. B **62**, 7901 (2000).
[31] Shang-Di Mo and W. Y. Ching, Appl. Phys. Lett. **78**, 3809 (2001).
[32] W. Y. Ching, Shang-Di Mo, and Yu Chen, J. Am. Ceram. Soc. **85**, 11 (2002).
[33] S. Aryal, P. Rulis, and W. Y. Ching, Am. Mineral. **93**, 114 (2008).
[34] T. Mizoguchi, K. Tatsumi, and I. Tanaka, Ultramicroscopy **106**, 1120 (2006).
[35] Y. Chen, S. D. Mo, M. Kohyama, H. Kohno, S. Takeda, and W. Y. Ching, Mater. Trans. **43**, 1430 (2002).
[36] I. Tanaka, T. Mizoguchi, M. Matsui, S. Yoshioka, F. Oba, H. Adachi, T. Okajima, M. Umesaki, W. Y. Ching, Y. Inoue, M. Mizuno, and Y. Shirai, Nat. Mater. **2**, 541 (2003).
[37] T. Mizoguchi, T. Sasaki, S. Tanaka, K. Matsunaga, T. Yamamoto, M. Kohyama, and Y. Ikuhara, Phys. Rev. B **74**, 235408 (2006).
[38] P. Rulis, W. Y. Ching, and M. Kohyama, Acta Mater. **52**, 30009 (2004).
[39] A. Zerr, G. Miehe, G. Serghiou, M. Schwarz, E. Kroke, R. Riedel, H. Fueβ, P. Kroll, and B. Boehler, Nature (London) **400**, 340 (1999).
[40] S. D. Mo, L. Ouyang, W. Y. Ching, I. Tanaka, Y. Koyama, and R. Riedel, Phys. Rev. Lett. **83**, 5046 (1999).
[41] T. Suga, T. Mizoguchi, M. Kunisu, K. Tatsumi, T. Yamamoto, I. Tanaka, and T. Sekine, Mater. Trans. **45**, 2039 (2004).
[42] M. Gülgün, W. Y. Ching, Y.-N. Xu, and M. Rühle, Philos. Mag. B **79**, 921 (1999).
[43] S. Köstlmeier and C. Elsässer, Phys. Rev. B **60**, 14025 (1999).
[44] W. Y. Ching, Ming-Zhu Huang, and Shang-Di Mo, J. Am. Ceram. Soc. **83**, 780 (2000).
[45] P. A. Lee and G. Beni, Phys. Rev. B **15**, 2862 (1977).
[46] P. Schattschneider, Ultramicroscopy **28**, 1 (1989).
[47] D. A. Muller, D. J. Singh, and J. Silcox, Phys. Rev. B **57**, 8181 (1998).
[48] *Unoccupied Electronic States, Fundamentals for XANES, EELS, IPS and BIS*, edited by J. C. Fuggle and J. E. Inglesfield (Springer-Verlag, New York, 1992).
[49] J. J. Rehr and R. C. Alberts, Rev. Mod. Phys. **72**, 621 (2000).
[50] I. Tanaka, T. Mizoguchi, and T. Yamamoto, J. Am. Ceram. Soc. **88**, 2013 (2005).
[51] P. A. M. Dirac, Proc. R. Soc. London, Ser. A **114**, 243 (1927).
[52] W. Y. Ching, J. Am. Ceram. Soc. **73**, 3135 (1990).
[53] H. P. Hjalmarson, H. Buttner, and J. D. Dow, Phys. Rev. B **24**, 6010 (1980).
[54] P. J. W. Weijs, M. T. Czyzyk, J. F. van Acker, W. Speier, J. B. Goedkoop, H. van Leuken, H. J. M. Hendrix, R. A. de Groot, G. van der Laan, K. H. J. Buschow, G. Wiech, and J. C. Fuggle, Phys. Rev. B **41**, 11899 (1990).
[55] I. Tanaka and H. Adachi, Phys. Rev. B **54**, 4604 (1996).
[56] J. Zannen, G. A. Sawatzky, J. Fink, W. Speier, and J. C. Fuggle, Phys. Rev. B **32**, 4905 (1985).
[57] E. Tamura, J. van Ek, M. Fröba, and J. Wong, Phys. Rev. Lett. **74**, 4899 (1995).
[58] P. Hohenberg and W. Kohn, Phys. Rev. **136**, 864 (1964).
[59] W. Kohn and L. J. Sham, Phys. Rev. **140**, A1133 (1965).
[60] Th. Lindner, H. Sauer, W. Engel, and K. Kambe, Phys. Rev. B **33**, 22 (1986).
[61] J. Robertson, Phys. Rev. B **28**, 3378 (1983).
[62] K. Matsunaga, T. Mizouguchi, A. Nakamura, T. Yamamoto, and Y. Ikuhara, Appl. Phys. Lett. **84**, 4795 (2004).
[63] T. Suga, S. Kameyama, S. Yoshioka, T. Yamamoto, I. Tanaka, and T. Mizoguchi, Appl. Phys. Lett. **86**, 163113 (2005).
[64] K. Kimoto, Y. Matsui, T. Nabatame, T. Yasuda, T. Mizoguichi, I. Tanaka, and A. Toriumi, Appl. Phys. Lett. **83**, 4306 (2003).
[65] T. Mizoguchi, M. Sakurai, A. Nakamura, K. Matsunaga, I. Tanaka, T. Yamamoto, and Y. Ikuhara, Phys. Rev. B **70**, 153101 (2004).
[66] K. Tatsumi, T. Mizoguchi, S. Yoshioka, Yamamoto, T. Suga, T. Sekine, and I. Tanaka, Phys. Rev. B **71**, 033202 (2005).
[67] J. A. Soininen and E. L. Shirley, Phys. Rev. B **64**, 165112 (2001).
[68] A. J. Scott, R. Brydson, M. MacKenzie, and A. J. Craven, Phys. Rev. B **63**, 245105 (2001).

[69] K. van Benthem, C. Elsasser, and M. Ruhle, Ultramicroscopy **96**, 509 (2003).
[70] M. Launay, F. Boucher, and P. Moreau, Phys. Rev. B **69**, 035101 (2004).
[71] V. Krayzman, I. Levin, J. C. Woicik, D. Yoder, and D. A. Fisher, Phys. Rev. B **74**, 224104 (2006).
[72] D. Cabaret, F. Mauri, and G. S. Henderson, Phys. Rev. B **75**, 184205 (2007).
[73] G. E. Brown, Jr., G. A. Waychunas, J. Stohr, and F. Sette, J. Phys. Colloq. **47**, 685 (1986).
[74] D. Li, G. M. Bancroft, M. Kasrai, M. E. Fleet, X. H. Feng, K. H. Tan, and B. X. Yang, Solid State Commun. **87**, 613 (1993).
[75] D. Wallis, P. H. Gaskell, and R. Brydson, J. Microsc. **180**, 307 (1993).
[76] T. Sharp, Z. Wu, F. Feifert, B. Poe, M. Doerr, and E. Paris, Phys. Chem. Miner. **23**, 17 (1996).
[77] B. Poe, F. Seifert, T. Sharp, and Z. Wu, Phys. Chem. Miner. **24**, 477 (1997).
[78] Z. Y. Wu, F. Jollet, and F. Seifert, J. Phys.: Condens. Matter **10**, 8083 (1998).
[79] L. A. J. Garvie and P. R. Buseck, Am. Mineral. **84**, 946 (1999).
[80] A. V. Soldatov, M. Kasrai, and G. M. Bancroft, Solid State Commun. **15**, 687 (2000).
[81] Y.-N. Xu and W. Y. Ching, Phys. Rev. B **59**, 10530 (1999).
[82] W. Y. Ching and Yong-Nian Xu, Phys. Rev. B **59**, 12815 (1999).
[83] F. de Groot, Chem. Rev. (Washington, D.C.) **101**, 1779 (2001).
[84] K. Ogasawara, T. Iwata, Y. Koyama, T. Ishii, I. Tanaka, and H. Adachi, Phys. Rev. B **64**, 115413 (2001).
[85] S. J. L. Billinge and I. Levin, Science **316**, 561 (2007).